Method for Experimental Study of Circuits with Triple Modal Reservation in Time and Frequency Domains

Valeriy P. Kosteletskii
dept. of television and control
Tomsk State University of Control Systems and Radioelectronics
Tomsk, Russian Federation
0000-0003-1275-6406

Artem V. Medvedev
dept. of television and control
Tomsk State University of Control Systems and Radioelectronics
Tomsk, Russian Federation
0000-0003-4718-1024

Yevgeniy S. Zhechev
dept. of television and control
Tomsk State University of Control Systems and Radioelectronics
Tomsk, Russian Federation
0000-0003-4469-7033

***Abstract*—The paper presents a new method for experimental studies of typical prototypes with triple modal reservation. The authors propose to define the investigated devices in the frequency domain and then by using Advanced Design System software to redefine their characteristics in the time domain. The paper contains recommendations for the preparation and conduction of such experimental studies. Using these recommendations, the authors conducted measurements of the complex *S*-parameters of the circuits with triple modal reservation in the frequency range from 10 MHz to 18 GHz before and after failures. Then, to analyze the response to ultra-wideband interference, a pulse in the trapezoidal waveform with a duration of 150 ps was excited in Advanced Design System to the input of the reserved circuit. The maximum amplitude value at the end of the reserved circuit is obtained for all the faults studied. The authors also present the optimal order of switching the reserving circuits. This paper proposes the methods for analyzing the frequency and time characteristics. It makes possible to analyze the characteristics of circuits with multiple modal reservation and to determine the optimal switching order for reserving circuits. The proposed method requires commonly used equipment and a minimum set of technical tools that can reduce economic expenditures and time costs.**

Keywords—electromagnetic compatibility, ultra-short pulse, modal reservation, experimental method, multiconductor transmission lines

I. INTRODUCTION

Currently, the field of application of radio-electronic equipment (REE) is quite wide: space equipment, telecommunications and electrical networks, financial and banking systems, production facilities, military bases, radar stations, and others [1]. Because of the increasing complexity of modern REE and the importance of their uninterrupted operation, developers place high requirements on them to ensure the reliability of systems and components. A common approach to increasing the reliability of the REE is to provide redundancy of its main and critically important components [2]. The main idea of redundancy is the use of additional tools and capabilities to maintain the operable state of an object in case of failure of one or more of its elements [3]. The idea of redundancy is based on the replacement of a faulty element with a functioning one that is in reserve. There are two types of redundancy: cold and hot. The principle of cold redundancy is that the redundant elements do not carry the load until they are connected in place of the failed main element [4]. However, implementing this idea often becomes quite difficult if it is necessary to provide minimum time of transition to a redundant element and a minimum cost of equipment to ensure of failure-free operation for a certain time. In addition, the mass of the final product limits the use of such a method, which increases its cost [5].

An increase in operation frequency, mounting density, and a number of interconnections of REE leads to an increase in its susceptibility to electromagnetic interference (EMI). Particularly dangerous EMI are ultra-short pulses (USP) of sub-nanosecond duration, which propagate through electrical circuits by conductive way. The USP impact on electronic systems can be significant despite its small energy. In [6] it is shown that the level of destructive excitation for equipment is determined by the energy in a particular frequency range. There are structures in place to protect against USP that have a number of advantages as compared to commonly used protective devices. In such devices, USP propagates through an active conductor in an *N*-conductor line with inhomogeneous dielectric filling. During its propagation, the pulse is subject to modal distortions and decomposes into *N* pulses of lower amplitudes because of the difference of modal delays in the line [7]. Noteworthy is that the implementation of protection based on such devices may not need a separate protective device, but uses the interconnections already present on the printed circuit board (PCB).

Modal reservation (MR) allows to increase reliability and noise immunity of REE [8]. MR uses cold redundancy and modal filtering together. In the case of circuits with MR, modal filtering is maintained even if one of the conductors fails. After a conductor fails, there is a switch to another conductor [9]. The ratio of MR is determined by the number of reserving conductors. Now, in addition to single MR, there are double MR as well as triple MR [10]. Typical structures for implementing triple MR have been proposed: multiconductor transmission lines (MCTL). The order of switching after failures and the identification of the best configuration of parameters were investigated in [11].

However, so far, there is no method for conducting laboratory experiments to test typical prototypes with triple MR. Meanwhile, their development is necessary, because this type of reservation has its specifics, comprising the

The reported study was funded by Russian Science Foundation (project №20-19-00446) in TUSUR.

number of reserve conductors and features of the MCTL cross-section. In complementary fashion, early studies of MCTL with triple MR demonstrate the importance of switching order due to different inductive and capacitive coupling between the conductors. Thus, the aim of this paper is to develop a method for analyzing the frequency and time characteristics of circuits with triple MR before and after failures, as well as to validate it.

II. Devices Devinition With Triple MR in the Frequency Domain

This Section considers obtaining the frequency responses of the prototype with a triple MR before and after failures.

Fig. 1 shows the connection diagram as well as the cross-section of the prototype, where In. *N* and Out. *N* are the SMA connector at the near end far of the structure, respectively, Cond. *N* is the conductor number. Cross-section parameters: the width of conductors $w = 185$ μm and the thickness $t = 35$ μm, the gap between conductors $s = 315$ μm, the dielectric core thickness $h_1 = 600$ μm, the thickness of prepreg $h_2 = 130$ μm, the dielectric constants of core and prepreg $\varepsilon_{r1} = 4.3$, $\varepsilon_{r2} = 10.2$, respectively.

The structure is considered to operate until failure if matched loads of 50 Ω (*R*) are connected to the near and far ends of all conductors. The prototype is symmetrical in the cross-section, hence the *S*-parameters of possible conductor failure combinations are pairwise the same. Thus, there is no need to repeat the measurement for same cases. Based on this property of the prototype, Cond. 1. is used as the active conductor before failures. To simulate a conductor failure we used an open-circuit (OC) and a short-circuit (SC) loads.

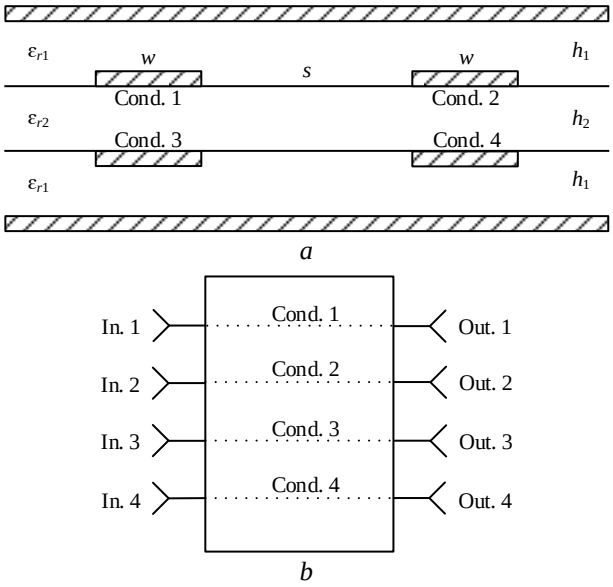

Fig. 1. Cross-section (*a*) and connection diagram (*b*) of the prototype with triple MR.

To identify the optimal order of conductor switching it is necessary to obtain sets of *S*-parameters and time responses for the required variants of terminations, namely before and after failure, under different failure variants. Table I shows failure variants in the structure with triple MR. Fig. 2 shows connection diagram for measuring the *S*-parameters of DUT.

TABLE I. Failure Options For Structures With Triple MR

Option	After failure 1	Measurement number	Option	After failure 2	Measurement number	After failure 3 (for all options)	Measurement number
1	*R*-OC, *R*-*R*, *R*-*R*	1	1	*R*-OC, *R*-OC, *R*-*R*	7	*R*-OC, *R*-OC, *R*-OC	31
						R-OC, OC-*R*, *R*-OC	32
				R-OC, OC-*R*, *R*-*R*	8	*R*-OC, *R*-SC, *R*-OC	33
				R-OC, *R*-SC, *R*-*R*	9	*R*-OC, SC-*R*, *R*-OC	34
				R-OC, SC-*R*, *R*-*R*	10	*R*-SC, *R*-SC, *R*-OC	35
						R-SC, SC-*R*, *R*-OC	36
	R-SC, *R*-*R*, *R*-*R*	2		*R*-SC, *R*-SC, *R*-*R*	11	*R*-SC, *R*-OC, *R*-OC	37
				R-SC, SC-*R*, *R*-*R*	12	*R*-SC,OC -*R*, *R*-OC	38
				R-SC, *R*-OC, *R*-*R*	13	*R*-OC, *R*-OC, *R*-SC	39
				R-SC, OC-*R*, *R*-*R*	14	*R*-OC, OC-*R*, *R*-SC	40
						R-OC, *R*-SC, *R*-SC	41
2	*R*-*R*, *R*-OC, *R*-*R*	3	2	*R*-*R*, *R*-OC, *R*-OC	15	*R*-OC, SC-*R*, *R*-SC	42
				R-*R*, *R*-OC, OC-*R*	16	*R*-SC, *R*-SC, *R*-SC	43
				R-*R*, *R*-OC, *R*-SC	17	*R*-SC, SC-*R*, *R*-SC	44
				R-*R*, *R*-OC, SC-*R*	18	*R*-SC, *R*-OC, *R*-SC	45
						R-SC, OC-*R*, *R*-SC	46
	R-*R*, *R*-SC, *R*-*R*	4		*R*-*R*, *R*-SC, *R*-SC	19	*R*-OC, *R*-OC, SC-*R*	47
				R-*R*, *R*-SC, SC-*R*	20	*R*-OC, OC-*R*, SC-*R*	48
				R-*R*, *R*-SC, *R*-OC	21	*R*-OC, *R*-SC, SC-*R*	49
				R-*R*, *R*-SC, OC-*R*	22	*R*-OC, SC-*R*, SC-*R*	50
						R-SC, *R*-SC, SC-*R*	51
3	*R*-*R*, *R*-*R*, *R*-OC	5	3	*R*-OC, *R*-*R*, *R*-OC	23	*R*-SC, SC-*R*, SC-*R*	52
				OC-*R*, *R*-*R*, *R*-OC	24	*R*-SC, *R*-OC, SC-*R*	53
				R-SC, *R*-*R*, *R*-OC	25	*R*-SC, OC-*R*, SC-*R*	54
				SC-*R*, *R*-*R*, *R*-OC	26	*R*-OC, *R*-OC, OC-*R*	55
						R-OC, OC-*R*, OC-*R*	56
	R-*R*, *R*-*R*, *R*-SC	6		*R*-SC, *R*-*R*, *R*-SC	27	*R*-OC, *R*-SC, OC-*R*	57
						R-OC, SC-*R*, OC-*R*	58
				SC-*R*, *R*-*R*, *R*-SC	28	*R*-SC, *R*-SC, OC-*R*	59
				R-OC, *R*-*R*, *R*-SC	29	*R*-SC, SC-*R*, OC-*R*	60
				OC-*R*, *R*-*R*, *R*-SC	30	*R*-SC, *R*-OC, OC-*R*	61
						R-SC, OC-*R*, OC-*R*	62

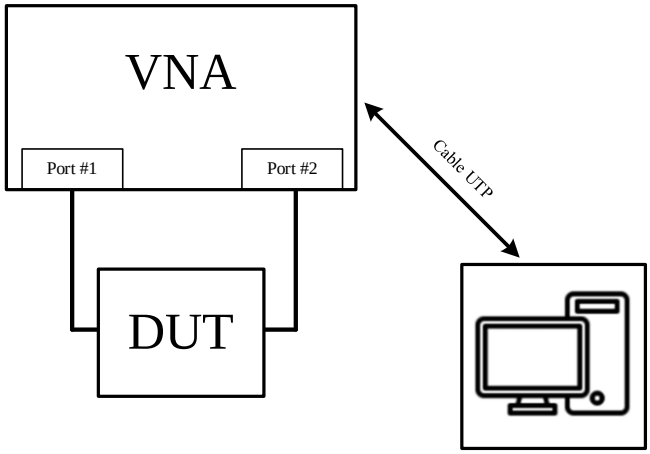

Fig. 2. Measurement setup for analyzing the *S*-parameters of the prototype.

To obtain the *S*-parameters of the prototype with triple MR, it is necessary to do the following:

- Prepare the measuring equipment and calibrate it according to the manual.
- Measure the frequency characteristics before failure: "Port 1" connect to "In. 1", "Port 2" connect to "Out. 1". Connect *R* to the free SMA connectors (6 pcs.). Measure the *S*-parameters.
- Measure the frequency characteristics after failures: "Port 1" connect to "In. 1", "Port 2" connect to "Out. 1". Next, on the SMA connectors "In. N" and "Out. N" by connecting SC, OC, and *R*, it is necessary to create the termination loads in accordance with the failure variants for the structures. Failure options are given in Table I. Measure the *S*-parameters.
- Save the obtained data in s2p format, the measurement number must correspond to the termination loads at the near and far conductors ends Cond. 2, Cond. 3, Cond. 4.

III. Devices with Triple MR in the Time Domain

This Section considers obtaining the time responses of the prototype with a triple MP before and after failures.

After the device was defined in the frequency domain, we can proceed to the analysis of its time characteristics. There are a number of approaches to determine the time characteristics of linear and nonlinear devices from their frequency characteristics [12–14]. In addition, for example, in [15], the authors presented a method for determining transients in the interconnections of integrated circuits. The time response was determined experimentally and is expressed as a parameter function in the frequency domain. After that, using the inverse Fourier transform, the exact form of the signal was determined. In [16], the authors presented a numerical method for converting S-parameters into a model in the time domain. At the same time, ordinary differential equations were solved. The approach used in [17] is also noteworthy, where the authors obtained time and frequency characteristics in the ADS system on the basis of experimentally determined *S*-parameters of a coupling microstrip TL.

After the prototype device was measured in the frequency range, as in [17], an analysis of the time characteristics in the ADS 2020 system was carried out. The prototype defined in the frequency domain was represented as an *n*-port device together with equations defining the relationship between the spectral variables of each port. Since the parameters of the scattering matrix were determined only for the reserved circuit on the circuit in the ADS 2020 system, the prototype under study was considered as a two-port device. A diagram for modeling the device in the time domain in the ADS system is shown in Fig. 3.

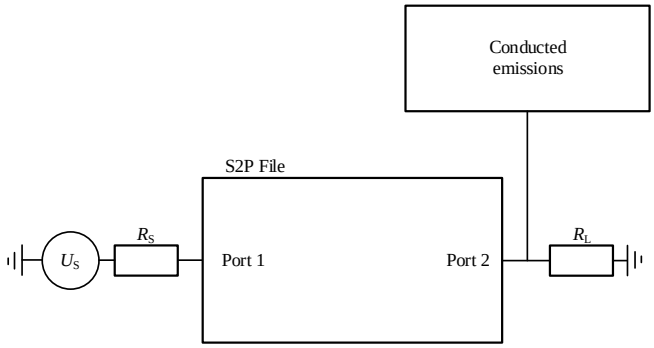

Fig. 3. Circuit for simulating the device with triple MR in the time domain in the ADS.

To evaluate the noise suppression characteristics of the device before and after failures, it is necessary to feed a USP that meets the requirements of the electromagnetic compatibility standard [18] to Port 1. The response to the given impact is observed in Port 2. To get it, you need to follow these steps:

- In the ADS system, perform the s2p import of S-parameters corresponding to the options before and after failures from Table II.
- Create a simulation model for calculating the response (shown in Fig. 3).
- Set the form of excitation, time step and total calculation time.
- Calculate the response to a given excitation.
- Visualize the response with the built-in tools you need for charting.
- Calculate and evaluate the amplitudes of decomposition pulses at the end of the reserved conductor (Port 2) using an analytical model for the case of complete matching, partial mismatch, or complete mismatch of the device with the path.
- Calculate and evaluate the *N*-norms (Table II) of the decomposed pulses at the end of the reserving conductor for various failure scenarios.

N-norms are used to characterise the signal in the time domain and to determine the susceptibility limits of the equipment [19]. *N*-norms are effectively applied to structures with single and triple MR [20, 21]. Table II shows the analyzed norms and their characteristics from [22]. Thus, for example, with their help, the possibility of electrical breakdown of a dielectric, burnout of an electronic component, etc. is estimated. In the formula, $U(t)$ refers to the voltage waveform of the decomposed pulses.

TABLE II. *N*-NORMS DESCRIPTIONS AND APPLICATIONS

Norm	Name	Equation	Application
N_1	Peak value (absolute)	$\lvert U(t)\rvert_{\max}$	Electric breakdown / circuit upset / arc-over effects
N_2	Peak derivative (absolute)	$\left\lvert \frac{dU(t)}{dt} \right\rvert_{\max}$	Component arcing / circuit upset
N_3	Peak pulse (absolute)	$\left\lvert \int_0^1 U(t)dt \right\rvert_{\max}$	Dielectric puncture (if U denotes E field)
N_4	Rectified general pulse	$\int_0^\infty \lvert U(t)\rvert\, dt$	Equipment damage
N_5	Square root of the action integral	$\left\{ \int_0^\infty \lvert U(t)\rvert^2\, dt \right\}^{\frac{1}{2}}$	Component burnout

*$U(t)$ is the voltage waveform of the USP on Port 2

IV. VALIDATION OF THE METHODS

The frequency range of the measured frequency response before failure ($|S_{21}|$, $|S_{11}|$, $|S_{12}|$ and $|S_{22}|$) is 10 MHz to 18 GHz. In the following, only $|S_{21}|$ and $|S_{12}|$ are considered, as only the bandwidth of bandwidth of a given device. Since it has complete reciprocity (amplitude, phase, frequency) per pass, the $|S_{21}|$ and $|S_{12}|$ characteristics are identical. Fig. 4 shows the frequency dependence of $|S_{21}|$ on failures, obtained in the course of the experimental study. The investigated structure with MR is a low-pass filter (LPF). The waveform of the envelope transfer characteristic of the structure is due to the dimensions and electrical structure parameters. Fig. 5 shows the time response to a total pulse duration of 0.15 ns with e.m.f. of 2 V obtained experimentally. At the far end of the structure with MR, 3 pulses are observed with an $U_{\max}$ of 159 mV, which is 6.3 times less than at the near end of the structure.

In accordance with the method, the frequency responses after failures were measured, and the obtained data were saved in the s2p format. Resulting in 62 *S*-parameter measurements after failures. Table III summarizes $U_{\max}$ for all after failure cases. Fig. 6 shows the frequency dependences $|S_{21}|$ in the range from 10 MHz to 1 GHz before and after failures (for the case of *R*–OC, SC–*R*, *R*–OC). Before failures first resonance frequency is 0.52 GHz, and for the case after failures it is 0.34 GHz. The bandwidths for the before and after failures is 0.053 and 0.064 GHz, respectively. Fig. 7 shows the time response at the far end of the structure before and after failures (for the case of *R*–OC, SC–*R*, *R*–OC).

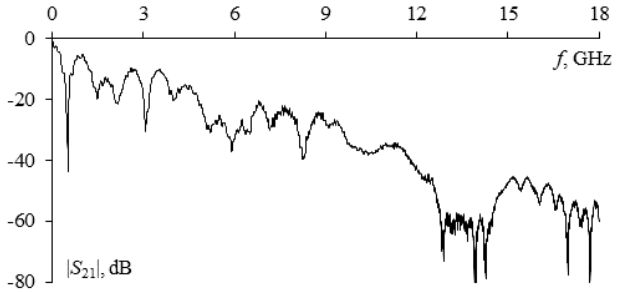

Fig. 4. Frequency dependence of $|S_{21}|$ up to 18 GHz for the structure before failures.

TABLE III. VALUES OF U_{MAX} AT THE END OF THE RESERVED CONDUCTOR AFTER VARIOUS FAILURE MODES

Option	After failure 1	$U_{\max}$, mV	Option	After failure 2	$U_{\max}$, mV	After failure 3 (for all options)	$U_{\max}$, mV
1	*R*-OC, *R*-*R*, *R*-*R*	157	1	*R*-OC, *R*-OC, *R*-*R*	156	*R*-OC, *R*-OC, *R*-OC	152
						R-OC, OC-*R*, *R*-OC	156
				R-OC, OC-*R*, *R*-*R*	155	*R*-OC, *R*-SC, *R*-OC	158
				R-OC, *R*-SC, *R*-*R*	157	*R*-OC, SC-*R*, *R*-OC	159
				R-OC, SC-*R*, *R*-*R*	158	*R*-SC, *R*-SC, *R*-OC	157
						R-SC, SC-*R*, *R*-OC	152
	R-SC, *R*-*R*, *R*-*R*	154		*R*-SC, *R*-SC, *R*-*R*	152	*R*-SC, *R*-OC, *R*-OC	150
				R-SC, SC-*R*, *R*-*R*	151	*R*-SC, OC-*R*, *R*-OC	157
				R-SC, *R*-OC, *R*-*R*	154	*R*-OC, *R*-OC, *R*-SC	151
				R-SC, OC-*R*, *R*-*R*	154	*R*-OC, OC-*R*, *R*-SC	152
						R-OC, *R*-SC, *R*-SC	154
2	*R*-*R*, *R*-OC, *R*-*R*	160	2	*R*-*R*, *R*-OC, *R*-OC	157	*R*-OC, SC-*R*, *R*-SC	151
				R-*R*, *R*-OC, OC-*R*	163	*R*-SC, *R*-SC, *R*-SC	153
				R-*R*, *R*-OC, *R*-SC	162	*R*-SC, SC-*R*, *R*-SC	158
				R-*R*, *R*-OC, SC-*R*	159	*R*-SC, *R*-OC, *R*-SC	151
						R-SC, OC-*R*, *R*-SC	152
	R-*R*, *R*-SC, *R*-*R*	158		*R*-*R*, *R*-SC, *R*-SC	159	*R*-OC, *R*-OC, SC-*R*	154
				R-*R*, *R*-SC, SC-*R*	157	*R*-OC, OC-*R*, SC-*R*	157
				R-*R*, *R*-SC, *R*-OC	163	*R*-OC, *R*-SC, SC-*R*	155
				R-*R*, *R*-SC, OC-*R*	160	*R*-OC, SC-*R*, SC-*R*	157
						R-SC, *R*-SC, SC-*R*	152
3	*R*-*R*, *R*-*R*, *R*-OC	161	3	*R*-OC, *R*-*R*, *R*-OC	156	*R*-SC, SC-*R*, SC-*R*	150
				OC-*R*, *R*-*R*, *R*-OC	155	*R*-SC, *R*-OC, SC-*R*	156
				R-SC, *R*-*R*, *R*-OC	155	*R*-SC, OC-*R*, SC-*R*	158
				SC-*R*, *R*-*R*, *R*-OC	157	*R*-OC, *R*-OC, OC-*R*	152
						R-OC, OC-*R*, OC-*R*	154
	R-*R*, *R*-*R*, *R*-SC	158		*R*-SC, *R*-*R*, *R*-SC	151	*R*-OC, *R*-SC, OC-*R*	157
						R-OC, SC-*R*, OC-*R*	155
				SC-*R*, *R*-*R*, *R*-SC	174	*R*-SC, *R*-SC, OC-*R*	157
				R-OC, *R*-*R*, *R*-SC	157	*R*-SC, SC-*R*, OC-*R*	152
				OC-*R*, *R*-*R*, *R*-SC	158	*R*-SC, *R*-OC, OC-*R*	150
						R-SC, OC-*R*, OC-*R*	156

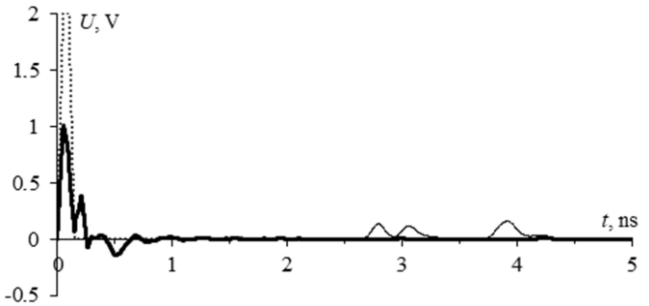

Fig. 5. E.m.f. voltage waveforms of the source (· · ·) at the near (▬) and far (—) ends of the structure before failures.

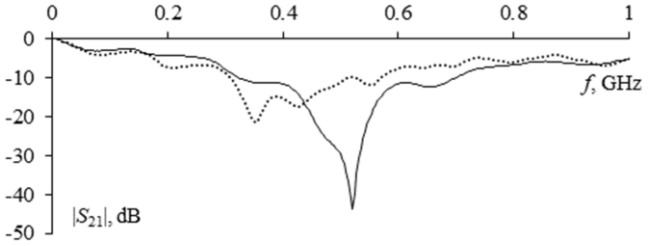

Fig. 6. Frequency dependencies $|S_{21}|$ for the structure before (—) and after (· · ·) failures

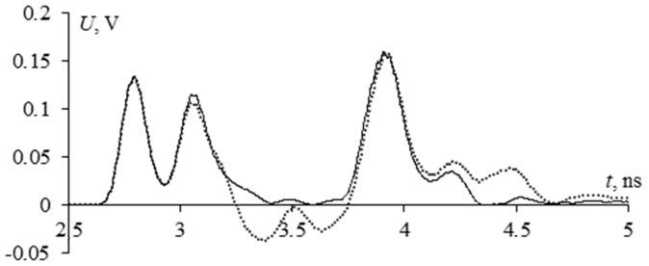

Fig. 7. Voltage waveforms at the far end of the structure before (—) and after (· · ·) failures

Table IV summarizes the analyzed norms and their characteristics used in the experiment. The experiment showed that before and after failures, the *N*1 norm does not significantly change, the difference is 0.6%. It means that the probability of circuit failure / electrical breakdown / arc effects before and after failures does not change. The *N*2 rate before and after failures increases by 41%. It implies that the probability of circuit failure / electric flashover / arc effects before and after failure increases. The *N*3 norm before and after failures is reduced by 2%. It suggests that the probability of dielectric breakdown before and after a failure is reduced. The norm *N*4 before and after failures increases by 9.5%. It implies that the probability of equipment damage before and after failure increases. The norm *N*5 before and after failures increases by 1.3%. It suggests that the likelihood of component burnout before and after failure increases.

TABLE IV. *N*-NORMS BEFORE AND AFTER FAILURES AT ONE OF THE ENDS OF THE RESERVING CONDUCTOR

	N1	**N2**	**N3**	**N4**	**N5**
Before failure	0.160	$4.45 \cdot 10^{9}$	$7.96 \cdot 10^{-11}$	$7.96 \cdot 10^{-11}$	$2.64 \cdot 10^{-6}$
After failure	0.158	$10.7 \cdot 10^{9}$	$7.65 \cdot 10^{-11}$	$9.63 \cdot 10^{-11}$	$2.71 \cdot 10^{-6}$

V. CONCLUSION

Thus, the paper proposes a novel, detailed methodology for measuring the frequency and time characteristics by means of an experimental study. The method is distinguished by the possibility to determine the optimum order of conductor switching in a triple MR prototype. Using a minimal set of technical equipment, such a technique provides an opportunity to obtain the characteristics of the considered structure and to determine the optimal order of conductor switching. The method was validated, and features of the triple MR before and after failures were revealed. To analyze how critical the effect of pulses of different duration on functional safety, *N*-norms were used to estimate the extent to which a high-power pulse can affect electronic equipment and components.

REFERENCES

[1] S. Vass, “Defense against electromagnetic pulse weapons,” Aarms, 2004, vol. 3, no. 3, pp. 443–457.

[2] K. C. Kapur, M. Pecht, Reliability Engineering, Wiley Interience, 2014, 512 p.

[3] Y. Li, H. Chen, J. Huang, X. Li, T. -Y. Zhang and H. -Z. Huang, “Reliability Allocation and Prediction for Command and Control System,” 2020 Global Reliability and Prognostics and Health Management (PHM-Shanghai), 2020, pp. 1-6.

[4] T. Jin, Reliability Engineering and Services. Wiley Interience, 2019.

[5] E. Ismail, N. Utelieva, A. Balmaganbetova and S. Tursynbayeva, “The choice of measures reliability of the software for space applications,” 2020 International Conference on Electrical, Communication, and Computer Engineering (ICECCE), 2020, pp. 1-5.

[6] W. A. Radasky, C. E. Baum and M. W. Wik, “Introduction to the special issue on high-power electromagnetics (HPEM) and intentional electromagnetic interference (IEMI),” in IEEE Transactions on Electromagnetic Compatibility, vol. 46, no. 3, pp. 314-321, Aug. 2004.

[7] A. O. Belousov, et. al., “From Symmetry to Asymmetry: The Use of Additional Pulses to Improve Protection against Ultrashort Pulses Based on Modal Filtration,” Symmetry, 2020, vol. 12(7), no. 1117, pp. 1–38.

[8] T. R. Gazizov, P. E. Orlov, A. M. Zabolotsky and S. P. Kuksenko, “New concept of critical infrastructure strengthening,” Proc. of the 13th Int. Conf. of Numerical Analysis and Applied Mathematics, pp. 1–3, 2015.

[9] A. V. Medvedev and T. R. Gazizov, “Studying the circuit switching order after failures for a shielded structure with triple modal reservation,” 2021 Ural Symposium on Biomedical Engineering, Radioelectronics and Information Technology (USBEREIT), 2021, pp. 0427-0430.

[10] V. R. Sharafutdinov and T.R. Gazizov, “Analysis of reservation methods based on modal filtration,” Systems of Control, Communication and Security, no. 3, pp. 117–144, 2019.

[11] A. O. Belousov, et. al., “Switching Order after Failures in Symmetric Protective Electrical Circuits with Triple Modal Reservation,” Symmetry, vol. 13(6), no. 1074, pp. 1–22, 2021.

[12] Z. Su and T. J. Brazil, “Discrete-time representation of band-pass frequency-domain data for Envelope Transient simulation,” 2010 IEEE MTT-S International Microwave Symposium, 2010, pp. 552-555.

[13] J. Schutt-Aine, J. Tan, C. Kumar and F. Al-Hawari, “Blackbox Macromodel with S-Parameters and Fast Convolution,” 2008 12th IEEE Workshop on Signal Propagation on Interconnects, 2008, pp. 1-4.

[14] Y. Wang and T. J. Brazil, “A comparison between discrete-time and vector fitting representations of s-parameter data,” in 2014 International Workshop on Integrated Nonlinear Microwave and Millimetre-wave Circuits (INMMiC). IEEE, 2014, pp. 1–3.

[15] Y. Eo, W. R. Eisenstadt, and J. Shim, “S-parameter-measurement-based high-speed signal transient characterization of VLSI interconnects on SIO2-SI substrate,” IEEE Transactions on Advanced Packaging, vol. 23, no. 3, pp. 470–479, 2000.

[16] J. M. Griffith and M. V. Toupikov, “Time-domain modeling from *S*-parameters: applicable to hard disk drives,” IEEE Transactions on Magnetics, vol. 39, no. 6, pp. 3581–3586, 2003.

[17] R. Vauché et al., “Experimental Time-Domain Study for Bandpass Negative Group Delay Analysis With Lill-Shape Microstrip Circuit,” in IEEE Access, vol. 9, pp. 24155-24167, 2021.

[18] IEC. 61000–1–5. “Electromagnetic compatibility (EMC) – Part 1–5: High power electromagnetic (HPEM) effects on civil systems. ” Ed: IEC, 2004.

[19] C. E. Baum, Norms and Eigenvector norms, Mathematics Notes 63, 1979, 42 p.

[20] Y. S. Zhechev, A. V. Zhecheva, A. V. Medvedev, and T. R. Gazizov, “Using N-norms for analysing a device with a single modal reservation,” Journal of Physics: Conference Series, vol. 1611, no. 012065, pp.1–6, Aug. 2020.

[21] Y. S. Zhechev, et. al., “Using N-Norms for Analyzing Symmetric Protective Electrical Circuits with Triple Modal Reservation,” Symmetry, vol. 13, no. 12, p. 2390, Dec. 2021.

[22] D. Giri, High-power electromagnetic radiators: nonlethal weapons and other applications. Cambridge, MA: Harvard University Press, 2004.